J Neuropathol Exp Neurol
Vol. 81, No. 9, September 2022, pp. 717–730
doi: 10.1093/jnen/nlac054

OXFORD

ORIGINAL ARTICLE

Apolipoprotein E ε4 Mediates Myelin Breakdown by Targeting Oligodendrocytes in Sporadic Alzheimer Disease

Gerald Wai-Yeung Cheng, MRes, Kingston King-Shi Mok, BSc, Sunny Hoi-Sang Yeung, BSc, Julia Kofler, MD, Karl Herrup, PhD, and Kai-Hei Tse, PhD

Abstract

White matter degradation in the frontal lobe is one of the earliest detectable changes in aging and Alzheimer disease. The ε4 allele of apolipoprotein E (*APOE4*) is strongly associated with such myelin pathology but the underlying cellular mechanisms remain obscure. We hypothesized that, as a lipid transporter, APOE4 directly triggers pathology in the cholesterol-rich myelin sheath independent of AD pathology. To test this, we performed immunohistochemistry on brain tissues from healthy controls, sporadic, and familial Alzheimer disease subjects. While myelin basic protein expression was largely unchanged, in frontal cortex the number of oligodendrocytes (OLs) was significantly reduced in *APOE4* brains independent of their Braak stage or NIA-RI criteria. This high vulnerability of OLs was confirmed in humanized *APOE3* or *APOE4* transgenic mice. A gradual decline of OL numbers was found in the aging brain without associated neuronal loss. Importantly, the application of lipidated human APOE4, but not APOE3, proteins significantly reduced the formation of myelinating OL in primary cell culture derived from *Apoe*-knockout mice, especially in cholesterol-depleted conditions. Our findings suggest that the disruption of myelination in APOE4 carriers may represent a direct OL pathology, rather than an indirect consequence of amyloid plaque formation or neuronal loss.

Key Words: Alzheimer disease, Amyloid-independent, APOE4, Lipid transport, Myelin, Oligodendrocyte.

INTRODUCTION

Extensive myelination in the frontal lobe is a prominent but late-maturing feature of the primate brain (1). Ironically, while the slow maturation process means that the frontal lobe white matter (WM) is not fully developed until well into the fourth decade of human life, frontal lobe WM is also one of the earliest structures to be lost during normal aging (2–6). The loss of myelin content is significant enough to be tracked by diffusion tensor imaging (DTI) (7–9), and such imaging studies have shown that the microstructural integrity of WM in most cerebral cortex regions, particularly in the frontal lobe, regresses with age even in healthy individuals. The importance of these changes is underscored by the additional finding that the loss of WM integrity exhibits a close relationship with declines in cognitive performance including memory, speed of processing, and reaction time (10–13). Not surprisingly, therefore, the natural loss of WM is significantly accelerated in individuals with cognitive impairment and sporadic Alzheimer disease (sAD) (3, 14, 15).

Apolipoprotein E is the strongest and most prevalent genetic risk factor for sAD (16). Based largely on the amyloid cascade hypothesis, the traditional view of the linkage between *APOE* and the risk of sAD centers on the role of the APOE protein as a carrier of the beta-amyloid (Aβ) peptide. While this idea has face validity, many amyloid-independent cellular mechanisms can equally well explain the linkage (17). The major role of APOE in the brain is to serve as the lipid carrier for cholesterol transport between astrocytes and other brain cell types. This raises the possibility that APOE may be essential for the formation and degradation of myelination. Myelin is one of the most lipid- and cholesterol-rich cellular structures in the human body and a high cholesterol content is a prerequisite for the maturation of the myelin-making oligodendrocyte (OL) (18–20). During aging, the OL population becomes less capable of intrinsic cholesterol synthesis. This

From the Department of Health Technology and Informatics, The Hong Kong Polytechnic University, Kowloon, Hong Kong SAR (GWYC, KKSM, SHSY, KHT); Division of Neuropathology, School of Medicine, University of Pittsburgh, Pittsburgh, Pennsylvania, USA (JK); Department of Neurobiology, School of Medicine, University of Pittsburgh, Pittsburgh, Pennsylvania, USA (KH).

Send correspondence to: Kai-Hei Tse, PhD, Department of Health Technology and Informatics, Lee Shau Kee Building, The Hong Kong Polytechnic University, 11 Yuk Choi Road, Hung Hom, Kowloon, Hong Kong SAR; E-mail: kh-franki.tse@polyu.edu.hk.

This study is supported by General Research Fund GRF16124916 (Research Grant Council, Hong Kong SAR) with KHT as the principal investigator. We acknowledge the kind support from Neuropathology Core of Alzheimer's Disease Research Center at University of Pittsburgh for the PPFE tissues. KH is supported by Start-up Fund at Department of Neurobiology, University of Pittsburgh and the Australian National Health and Medical Research Fund (APP1160691). Dr. Kofler and Alzheimer's Disease Research Center at the University of Pittsburgh are supported by National Institute on Aging (NIA) P30 AG066468 and NIA P50 AG005133. JK and KH receive additional support from the NIA (R01 AG069912).

The authors have no duality or conflicts of interest to declare.

Supplementary Data can be found at academic.oup.com/jnen.

makes an OL increasingly reliant on lipids transported from astrocytes (21, 22), and increases the importance of APOE as a cholesterol carrier. Due to its high lipid binding affinity, the ε4 allele of apolipoprotein E (APOE4) is less effective than the more common APOE3 allele to transport lipids between brain cells (17). Given these observations, there is likely a correlation between the observed loss of myelin in Alzheimer disease and an individual's APOE*4* genotype (23–26).

In Alzheimer disease, the earliest myelin loss happens at least a decade before the onset of cognitive symptoms or pathological deposition of misfolded proteins. Based on this timing, we and others have hypothesized that loss of myelin integrity is one of the initiating events of sAD (3, 14, 27). While attractive as a hypothesis given the abundant neuroimaging evidence (28, 29), the cell biology that might connect APOE and myelin remains unknown, especially the mechanisms underlying the high vulnerability of WM microstructure observed in *APOE4* carriers (23–26, 28, 29). We have recently shown that the dementia-associated loss of OLs, particularly mature OLs (mOL), is independent of amyloid plaque deposition (30). In the current report, we further segregate the pathogenic effects of *APOE4* and amyloid plaque deposition on OL population in a well-characterized cohort of sporadic and familial Alzheimer disease (fAD). We find that APOE4 exerts intrinsic effects on the cell biology of the OL population that in turn contribute to the WM abnormalities found in sAD. Further, in vitro cell culture models, as well as in vivo studies with humanized mice carrying the human *APOE3* or *APOE4* gene in place of the endogenous mouse *Apoe* gene, provide additional evidence that the APOE4 protein is directly detrimental to OLs, especially myelinating OLs. The data further suggest that these effects are independent of both amyloid plaques and neuronal loss.

MATERIALS AND METHODS

Human Postmortem Brain Tissues

A cohort of formalin-fixed paraffin-embedded postmortem tissues from sAD (mean age = 83.0 years, n = 18), fAD (mean age = 50.3 years, n = 7) and age-matched healthy controls (NC, mean age = 78.0 years, n = 9) were kindly provided by Alzheimer's Disease Research Center (ADRC) Neuropathology Core at University of Pittsburgh with approvals from the Committee for Oversight of Research and Clinical Training Involving Decedents at University of Pittsburgh. The study of human tissue is also approved by the Institutional Review Board at The Hong Kong Polytechnic University (PolyU)—IRB (HSEARS20190809001). The basic neuropathology of all cases was characterized and classified by Braak staging (31) and Institute on Aging and Reagan Institute (NIA-RI) diagnosis criteria (32).

Animal Subjects

Homozygous hAPOE3 (RBRC03390, B6; 129-Apoe$^{<tm>/3SfuRbrc}$) and hAPOE4 (RBRC03418 B6; 129-Apoe$^{<tm(APOE4)Sfu>/SfuRbrc}$) knock-in mice were obtained from RIKEN BioResource Research Center, Japan; Apoe-knockout mice (*Apoe*-KO; *Apoe*$^{-/-}$; *Apoe*^{tm1Unc}) were obtained from The Jackson Laboratory (Bar Harbor, ME). These mice were originally developed by Shinobu Fujita at the Mitsubishi Kagaku Institute of Life Sciences (33), and backcrossed to C57BL/6 background. In both strains, the mouse *Apoe* gene locus flanking part of exon 2, the entire exon 3 and most of the exon 4 is replaced by a human *APOE3* or *APOE4* cDNA with a floxed neomycin cassette. The colonies were maintained by crossing heterozygotes. In all cases, wild-type mice generated in these crosses served as controls. All animals were housed in a temperature- and humidity-controlled environment on a 12-hour light/dark cycle with food and water ad libitum. All mice were kept and cared for at Centralized Animal Facilities at The Hong Kong Polytechnic University (PolyU) in compliance with the Ordinance and The Code of Practice for Care and Use of Animals for Experimental Purposes of Hong Kong. All animal experiments and analysis were approved and Animal Subjects Ethics Sub-Committee at PolyU. All experiments involving animals were performed under a valid license from the Department of Health in Hong Kong.

To isolate brain tissues, animals were deeply anesthetized by Avertin (1.25% tribromoethanol, 375 mg/kg, intraperitoneal, Sigma-Aldrich, St. Louis, MO) before transcardial perfusion with phosphate buffered saline (PBS) using a peristaltic pump. The whole brain was isolated by dissection. The left hemisphere was snap frozen for protein analysis and the right hemisphere was fixed by immersion in paraformaldehyde (4%, for 24 hours at 4°C). The brain tissue was then cryopreserved in PBS-sucrose (30% w/v for at least 48 hours at 4°C) and then embedded for cryosectioning in the sagittal plane at 10 μm, beginning at the midline. All sections were mounted on glass slides, dried, and kept at −80°C until use.

APOE Genotyping

APOE genotyping was performed after the completion of the histology studies. The genomic DNA from the postmortem human brain tissue was genotyped for *APOE* alleles E2, E3 or E4 using SYBR green-based real time polymerase chain reaction (PCR) as described by Calero et al (34, 35). All PCR-based *APOE* genotyping was further validated by immunohistochemistry using a specific monoclonal mouse antibody against the human APOE4 protein (Clone 4E4, MABN43, Millipore, Temecula, CA [36, 37]; 1:1000, antigen retrieval: ER1 solution, 20 minutes) as well as a rabbit monoclonal antibody against human APOE4 (Clone EPR24181-64, ab279714, Abcam, Cambridge, UK; 1:1000, antigen retrieval: ER2 solution, 20 minutes) on a Leica fully automated BOND-RX Multiplex tissue stainer with BOND Polymer Refine Detection Kit (Leica Biosystems, Lincolnshire, IL). The slides were reviewed and graded by 3 independent experimenters blinded to the case identity. In automated clinical immunoassay for APOE4, the use of clone 4E4 antibody demonstrated a sensitivity of ≥100%, specificity of ≥94.8%, and an accuracy ≥97.4% (36, 37). The specificity of each APOE4 antibody was verified against human APOE3 (rhAPOE3, #4699-100 BioVision, Waltham, MA) and recombinant human APOE4 (rhAPOE4, #4696-100, BioVision) by immunoblotting.

Conventional Immunohistochemistry

Paraffin sections of human frontal cortex, cerebellar cortex, brainstem, and hippocampus were examined. All tissues slides were incubated for 1 hour at 60°C prior to deparaffinization with xylene for 10 minutes followed by routine rehydration steps. Antigen retrieval was performed on the rehydrated tissues using basic Tris-EDTA buffer (10 mM Tris Base, 1 mM EDTA solution, 0.05% Tween 20, pH 9.0) at 100°C in a water bath for 30 minutes. After quenching the residual peroxidase activity with 3% H_2O_2, the specimens were blocked with normal donkey serum for 30 minutes and then the primary antibodies. The primary antibody, either myelin basic protein (MBP) (SMI-99P, 1:1000 Covance/BioLegend, San Diego, CA), Olig2 (MABN50, 1:300 Millipore), APC (Clone CC1, MABC200, 1:300, Millipore) or myelin regulatory factor (MyRF) (ABN45, 1:300, Millipore), was placed on the tissue overnight at 4°C. The sections were then washed and incubated with the corresponding secondary antibody of the DAB-based detection kits (VectaStain Elite ABC HRP Kit; DAB Peroxidase HRP Substrate Kit, Vector Laboratories, Burlingame, CA) according to the manufacturer's protocol. All sections were counter stained with Meyer hematoxylin, coverslipped, imaged on an upright microscope (BX53 with DP80 camera, Olympus, Tokyo, Japan), and scanned with a Leica Aperio CS2 digital pathology slide scanner (Leica Microsystems, Hong Kong SAR). To quantify the MBP staining, the overall myelin fiber intensity and subcortical WM area in the frontal cortex, whole slide images were quantified with QuPath software (38). For quantifications of cellular antigens, images with an area of 688.6 × 518.5 µm were acquired with a 20× objective. At least 10 random fields in the gray matter (GM) and WM of the frontal cortex were taken per case and analyzed by ImageJ (National Institute of Health, Bethesda, MD). The minimum of 1% area of the entire formalin-fixed paraffin-embedded postmortem specimen was sampled for each GM or WM sample (>3.57 mm^2).

Immunohistochemistry-Immunofluorescence

For mouse brain tissue, the washed sections were blocked with normal donkey serum (10%) in PBS containing Triton X-100 (0.3%, 1 hour, room temperature). Then tissues were incubated with specific primary antibodies overnight at 4°C. Following PBS washings, secondary antibodies conjugated with Alexa Fluor 488, 555 or 647 fluorochromes were applied to the section (Thermo Fisher Scientific, Waltham, MA) at room temperature for 1 hour. All nuclei were counterstained with 4′,6-diamidino-2-phenylindole (DAPI, Thermo Fisher Scientific) before mounting in Hydromount (National Diagnostics, Atlanta, GA) with coverslips. All tissue sections were examined on an upright microscope (BX53 with DP80 camera, Olympus) equipped with an X-Cite 120Q fluorescence illuminator and corresponding filters (Excelitas Technologies, Waltham, MA).

OL Cell Culture

For primary OL cultures, postnatal day 2 (P2) to P6 mouse pups were sacrificed by decapitation under deep hypothermal anesthesia, and brains extracted from the skull (39–41). After removal of the cerebellum and olfactory bulbs, all meninges were removed under a microscope. The whole cerebrum was then mechanically dissociated by fine scissors, and enzymatically dissociated by trypsin (0.25%, 30 minutes, 37°C, Gibco, Thermo Fisher Scientific). The neutralized cell suspension was filtered through a cell strainer with a 40 µm pore size. The suspension was then centrifuged (220 *g*, 5 minutes) with cell pellet resuspended and transferred to a dish coated with BSL1 (1:500, L1100, Vector Laboratories) to remove any isolectin $B4^+$ microglia. The resulting suspension, consisting primarily of a mixture of OL and astrocytes, was collected. For astrocyte culture, this suspension was placed on a 10 cm poly-L-lysine coated dish with complete DMEM. For OL culture, the cells plated on poly-L-lysine coated 60-mm culture dishes in growth medium composed of DMEM/F12 (Gibco, Thermo Fisher Scientific), normal horse serum ([NHS], 1% v/v, Thermo Fisher Scientific) and N2 supplement (bovine serum albumin [70 µg/mL], insulin [5 µg/mL], human transferrin [5 µg/mL], putrescine [1.6 µg/mL], progesterone [60 ng/mL], sodium selenite [5 ng/mL], and L-thyroxine [400 ng/mL], all from Sigma-Aldrich). Platelet-derived growth factor-AA ([PDGF], 10 ng/mL, Sigma-Aldrich), NT3 (1 ng/mL, Peprotech, East Windsor, NJ), and CNTF (10 ng/mL, Peprotech, NJ) were added to stimulate OL progenitor cell (OPC) proliferation. After 5 days of expansion, the OPCs were plated on coated 12 mm glass coverslips (50 000 cells each). To differentiate OPCs into mOLs, the cells were induced to differentiate for 7 days using 34 ng/mL triiodothyronine (T3) in the absence of growth factors, and at reduced NHS (0.1%) concentration. To study the effects of hAPOE, cholesterol and lipid transport on OLs, Lovastatin (3-hydroxy-3-methyl-glutaryl-coenzyme A reductase inhibitor, #1530, Tocris, Minneapolis, MN), with or without the addition of recombinant human APOE3 (rhAPOE3, #4699-100 BioVision) and recombinant human APOE4 (rhAPOE4, #4696-100, BioVision). To study lipidated rhAPOE3 and rhAPOE4, the recombinant proteins (4 µg/mL) were incubated normal horse serum (final concentration 0.1% v/v), which contains high cholesterol-rich lipids, for 30 minutes before application to the cultures. The use of cell culture serum to lipidated APOE proteins is an effective approach to test cholesterol transport, as reported recently (42). To study the effects of rhAPOE, the cells were fixed by 4% paraformaldehyde in PBS after 7 days in differentiation conditions for immunocytochemistry.

Immunocytochemistry

Cells were fixed with paraformaldehyde (4%, Sigma-Aldrich) for 20 minutes after washing with PBS. The cell membrane was permeabilized by 0.3% Triton X-100 containing normal donkey serum (5%) in PBS for 30 minutes. Primary antibodies against MAG (MAB1567, 1:500, Millipore), MBP (78896S, 1:500, Cell Signaling Technology, Danvers, MA), and Olig2 (Alexa fluor-488 conjugated, MABN50A4 1:500, Millipore) were applied sequentially followed by PBS washes and corresponding secondary antibodies conjugated with Alexa fluor-555 or -647. Samples without incubation with primary antibodies served as negative controls. The coverslips

were then imaged on a Nikon Ni-U Microscope equipped with DS-Qi2 monochrome camera and a pE-4000 white LED Illuminator with blue (Ex: 380/55), green (Ex: 470/30), red (Ex: 557/35), and far-red (Ex: 620/60) filters using a Nikon Plan Apo λ 20× Objective (N.A. 0.75, R.I. 1.0). To quantify, 5 images from random fields on each of 2 coverslips were captured from each specimen with Nikon NIS elements software (Nikon Instruments, Melville, NY). Each image covering an area of 0.778 mm^2 with an average of 1000 cells per image were analyzed by QuPath.

Immunoblotting

The left neocortex of each mouse brain tissue was used for extraction of proteins with RIPA buffer (radioimmunoprecipitation assay buffer, Millipore) supplemented with phosphatase and protease inhibitors (Roche, Hong Kong SAR). The protein concentrations were quantified with Bio-Rad Protein Assay (Bio-Rad, Hercules, CA). Normalized amounts of sample (20–50 μg proteins per lane) were electrophoresed on a 12% SDS-polyacrylamide gels and blotted to PVDF membranes. All nonspecific antibody binding was blocked by 5% nonfat milk. Primary antibody against MBP (SMI-99P, 1:3000, Covance/BioLegend), MOG (MAB5680, 1:3000, Millipore), MAG (MAB1567, 1:3000, Millipore), human APOE (Clone EP1374Y, ab52607, 1:500, Abcam), human APOE4 (Clone 4E4, MABN43, 1:500, Millipore), and GAPDH (Loading control, ab8245, 1:10 000, Abcam) were then applied. The probed membranes were incubated with horseradish peroxidase-linked secondary immunoglobulins (Cell Signaling Technology) before development with chemiluminescent substrates (SuperSignal West Pico or Dura, Thermo Fisher Scientific). The chemiluminescent signals were detected by medical grade films. The films were scanned for quantification using ImageJ.

Statistics

In each animal and cell culture studies, at least 3 independent experiments were conducted. All data in graphs are presented as mean value ± standard errors of the mean. In human tissue and animal experiments, unpaired t-tests were performed for comparisons between pairs. To test the differences of a single variable with equal variances, one-way analysis of variance (ANOVA) followed by Tukey post hoc tests were performed for comparisons between 3 or more groups in the human tissue and animal study (43). To test the smallest possible differences of 2 variables among groups in the cell culture, a two-way ANOVA was conducted followed by Fisher least significant difference (LSD) test. For testing differences in 3 independent groups ($k = 3$), Fisher LSD allows the computation of the smallest significant difference between 2 groups with a high power with little effects on Type I error (44–46). All statistical analyses were performed using GraphPad Prism software version 9.00 (GraphPad Software Inc., San Diego, CA). The statistical significance level was set as $p < 0.05$.

RESULTS

Intracortical Myelin Area Is Reduced With Increasing Braak Stage but Not With *APOE4* Genotype

We first investigated whether *APOE4*-mediated microstructural myelin changes were reflected histologically in postmortem human brain samples (Fig. 1A). This cohort included healthy controls (subjects with no cognitive deficit at death—NC) and subjects who had died with sAD or fAD. Regardless of clinical diagnosis, disease progression was evaluated by Braak staging (neurofibrillary tangle based) and NIA-RI diagnosis criteria (neurofibrillary tangle and neuritic plaque based). The *APOE* status was determined with PCR followed by histological confirmation using 2 APOE4-specific antibodies (Clone 4E4 and Clone EPR24181-64, Supplementary Data Fig. S1). The specificity of the 2 antibodies was validated by in-house testing using recombinant human APOE3 and APOE4 peptides (Supplementary Data Fig. S2). The Braak staging, NIA-RI-based diagnosis, and *APOE4* genotype for each case are described in Table. The percentage of *APOE4* carrier in Braak III-IV sAD, Braak V-VI sAD, Braak V-VI fAD were 55% (5/9), 33% (3/9), and 28% (2/7), respectively, and was 22% (2/9) in NC group (Table) and only 1 case was homozygous. The gross histology of all specimens revealed a well-demarcated cortical WM and GM with no significant difference in cortical thickness among Braak stages or *APOE* genotype (Fig. 1A, B). As anticipated from previous studies, immunohistochemistry of MBP revealed a significant reduction of intracortical myelin in advanced cases (Braak V-VI—sAD and fAD) (Fig. 1C). On the other hand, we found no difference in MBP signal intensity in *APOE4* carriers (Fig. 1B, C, right panels). The myeloarchitecture of the cortex was disrupted in specimens at advanced Braak stages (myeloarchitectural map; see [47]). We found that the light and dark bands of MBP staining were more torsional in their trajectory in severe sAD cases and were often distorted by abundant amyloid plaques or extracellular neurofibrillary tangles in fAD (Fig. 1D). Despite these morphological changes, the MBP signal intensity of the stained myelin fibers in the GM showed no differences among Braak stages nor with *APOE4* status (Fig. 1E, F). We did, however, find a small but significant reduction of MBP signal intensity in cortical WM in advanced sAD cases; no such change was found in *APOE4* carriers. At high magnification, the difference between NC, sAD, and fAD was clear especially in the thin and skewed fibers between cortical myelin layer 4–5 in the AD specimens (Fig. 1G). In fAD, the thickness and alignment of the myelin fibers were similar to NC, but the myelin fiber bundles were noticeably bent by the misfolded proteins that could be amyloid aggregations or extracellular neurofibrillary tangles, which appear as empty spaces in the micrograph.

Intracortical OLs Are Highly Vulnerable to *APOE4* Status but Not Braak Stage

The overall density of the OL population was then evaluated by immunostaining with the OL-specific transcription factor, Olig2. In frontal cortex, the $Olig2^+$ population showed

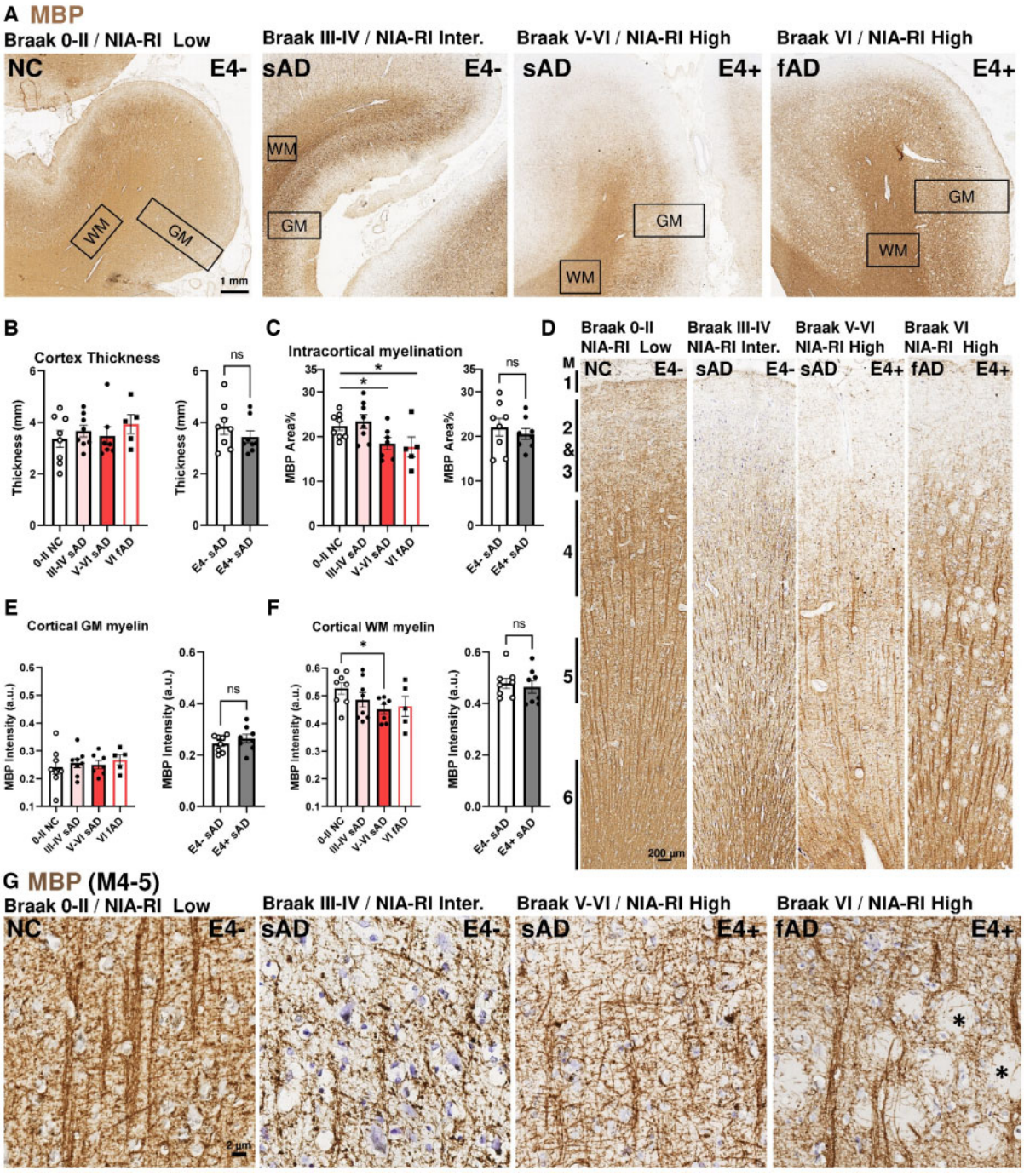

FIGURE 1. Myelin basic protein-expressing fibers are reduced in sAD frontal cortex independent of *APOE4* status. **(A)** Representative low-power micrograph of MBP immunohistochemistry on postmortem human frontal cortices from NC, sAD, and fAD. Braak stage of NFT or NIA-RI of NFT + NP are indicated on top left, APOE4 carrier status on top right; thicknesses of the GM and WM regions are indicated by rectangles. **(B)** No differences in the cortical GM thickness among groups by Braak stage or *APOE4* status in sAD cohorts. **(C)** Myelinated (MBP^+) areas of the GM are reduced in sAD and fAD with advanced Braak stages but are unaffected by *APOE4* status in sAD. **(D)** Representative mid-power images of the cortical GM showing the 6 layers of myeloarchitecture (M1-6) (47). **(E)** No differences in the MBP intensity among groups by Braak stage or *APOE4* status. **(F)** MBP intensity was reduced in sAD and fAD with Braak stage progression but unaffected by *APOE4* status. **(G)** High magnification between myelin layer 4-5. Strong, aligned, and organized MBP^+ myelin fibers were found in NC. The alignment and organization of MBP^+ fibers arrangements were disrupted in sAD; aligned fibers were deflected by amyloid plaques or extracellular neurofibrillary tangles (asterisks) in fAD. Statistical analyses by one-way ANOVA among groups with Tukey post hoc test, or unpaired t-test for pairwise comparison (*$p < 0.05$).

TABLE. Demographic and Neuropathology Details of Human Postmortem Tissues

Case	Age Group	Sex	*APOE4* Carrier	Braak Staging (NFT)	NIA-RI Dx Criteria (NFT+NP)	PMI (hours)
Age-matching normal controls (NC)						
NC1	86–90	M	−	II	N/A	3
NC2	81–85	M	−	I	Low likelihood	5
NC3	71–75	M	−	II	N/A	4.5
NC4	86–90	M	−	II	Low likelihood	7
NC5	61–65	M	−	N/A	N/A	6.5
NC6	76–80	M	+	II	N/A	6
NC7	76–80	F	−	II	Low likelihood	10.5
NC8	71–75	M	−	I	N/A	4.5
NC9	76–80	M	+	II	N/A	14
Sporadic Alzheimer disease (sAD)						
sAD1	86–90	M	+	III	Intermediate	9
sAD2	86–90	F	+	IV	Intermediate	6
sAD3	91–95	M	−	III	Intermediate	6
sAD4	76–80	M	+	IV	Intermediate	2
sAD5	86–90	M	+	IV	Intermediate	4
sAD6	81–85	M	−	IV	Intermediate	12
sAD7	76–80	M	+	IV	Intermediate	15
sAD8	86–90	M	−	IV	Intermediate	4
sAD9	76–80	M	−	IV	Intermediate	2
sAD1	86–90	M	−	VI	High likelihood	3
sAD2	71–75	M	+	VI	High likelihood	4
sAD3	76–80	F	−	VI	High likelihood	4
sAD4	76–80	F	−	VI	High likelihood	7.5
sAD5	81–85	M	−	VI	High likelihood	7
sAD6	86–90	M	−	V	High likelihood	2
sAD7	81–85	M	+	VI	High likelihood	4
sAD8	81–85	F	+	VI	High likelihood	2
sAD9	76–80	F	−	VI	High likelihood	3
Familial Alzheimer disease (fAD)						
fAD1	46–50	F	−	VI	High likelihood	10
fAD2	46–50	F	−	VI	High likelihood	18
fAD3	51–55	M	−	V	High likelihood	3
fAD4	51–55	M	+	VI	High likelihood	No record
fAD5	46–50	F	−	VI	High likelihood	6
fAD6	46–50	F	−	VI	High likelihood	6
fAD7	56–60	F	+	VI	High likelihood	9

Braak, Braak & Braak staging (31); NIA-RI, routine AD diagnosis by National Institute on Aging and Reagan Institute criteria (32); NFT, neurofibrillary tangle; NP, neuritic plaque; N/A, not applicable or detectable; +, *APOE4* Carrier; −, *APOE4* noncarrier; PMI, postmortem interval.

little change with Braak stage progression with high variations especially in the WM (Fig. 2A). By contrast, Olig2$^+$ cell density was significantly reduced in *APOE4* carriers. While the effect was evident in GM (56% reduction) it was even stronger in WM (82% reduction—Fig. 2B). The numbers of cells in the Olig2$^+$ subpopulation of mOLs were quantified based on their expression of the CC1 myelin marker. We found a significant reduction in CC1$^+$ cells in sAD at Braak III-IV compared to NC. The variability in Braak V-VI was substantial and may have obscured this difference (Fig. 2C, D). In *APOE4* carriers, the numbers of CC1$^+$ mOLs, like the number of Olig2$^+$ cells, were significantly reduced. In this case, however, the reduction seen in GM (58%) was nearly identical to that found in WM (51%) (Fig. 2D). MyRF is the master transcription factor that regulates the expression of key myelin genes. When found in the nucleus of an mOL, it can be used as a marker of an actively myelinating OL (48, 49). In cortical GM, unlike the situation with Olig2 and CC1, the MyRF$^+$ mOL population was significantly reduced with disease progression (Braak stage), and the *APOE* genotype was without effect (Fig. 2E, F). No significant changes in the density of MyRF$^+$ mOL were found. Next, we asked if the effects of *APOE4* on the OL population were found in other brain regions of the same subjects—cerebellum, brainstem, and hippocampus. While cerebellum demonstrated a significant reduction of the Olig2$^+$ OL population with Braak stages greater than II, the other

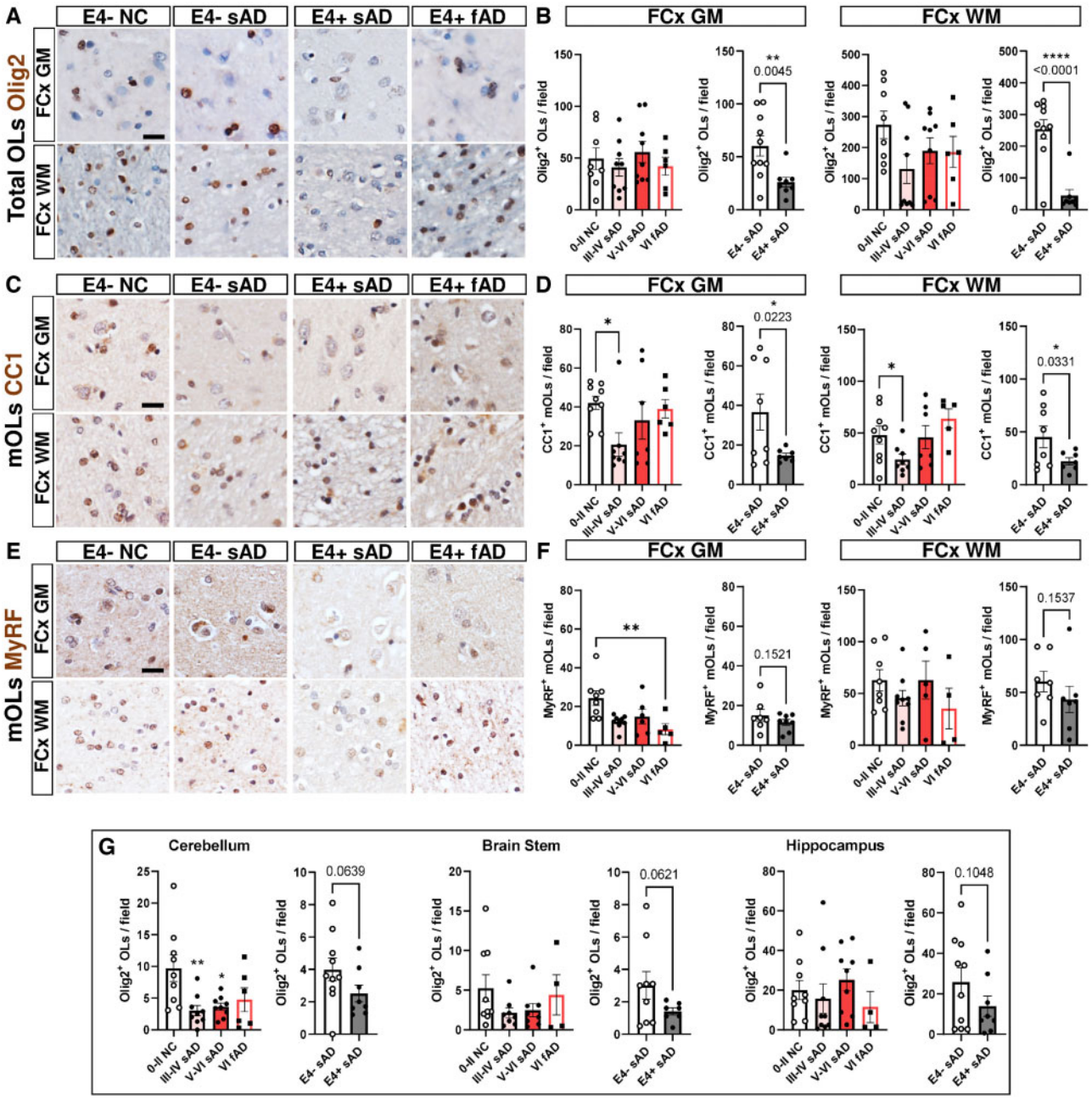

FIGURE 2. Oligodendrocytes are vulnerable to *APOE4* status but not Braak stage in frontal cortex. **(A–F)** Representative micrographs and quantifications of immunohistochemistry of OL in GM and WM of the frontal cortex among NC, sAD, and fAD cases. **(A, B)** Total OL populations were visualized and quantified by Olig2$^+$ cell staining (brown). No reduction was found among sAD and fAD of all Braak stages, but significant reductions of Olig2$^+$ OLs in both GM and WM were found in *APOE4* carriers among sAD cases. **(C, D)** The mOL populations were visualized and quantified by CC1$^+$ cell staining (brown). A significant reduction was only found in sAD at Braak III-IV but not in Braak V-IV or in fAD groups. A significant reduction of CC1$^+$ mOLs was also found in *APOE4* carriers in sAD in both GM and WM. **(E, F)** Mature and actively myelinating OL populations were visualized and quantified by MyRF$^+$ cell staining (brown). A significant reduction was only found in the fAD group; no differences were found in the *APOE4* carriers of the sAD group. **(G)** In the cerebellum, brainstem, and hippocampus, no significant changes of Olig2$^+$ OLs were found in any groups classified by Braak stages or *APOE4* status. The only exception was a significant reduction in the cerebellum of sAD groups. Statistical analysis by one-way ANOVA among groups with Tukey post hoc, or unpaired t-test between 2 groups (*$p < 0.05$, **$p < 0.01$, ****$p < 0.0001$, p value as indicated).

regions showed only a trend in this direction. A similar trend was found among the *APOE4* carriers but none of the reductions was statistically significant (Fig. 2G).

Human APOE Depletes OLs, but Not Myelin Fibers in the Aging Mouse Brain

We next examined transgenic knock-in mice expressing the human *APOE3* or *APOE4* allele in place of the endogenous mouse *Apoe* gene (33). hAPOE3 and hAPOE4 mice have been well characterized with respect to their altered cholesterol metabolism and blood brain barrier dysfunctions (33, 50–53). The altered expression of APOE in these 2 knock-in strains was first confirmed by immunoblotting using an antibody specific to human APOE (clone EP1374Y) and an antibody specific to human APOE4 isoform (clone 4E4) on mouse brain tissue lysates (Fig. 3A). At the predicted size of 34 kDa, a clear band of human APOE and human APOE4 was detected in all humanized strains (left) and hAPOE4 strain (right), respectively, with no detectable signals found in WT. The antigen specificity of clone 4E4 and EP1374Y was further confirmed against the recombinant human APOE3 and APOE4 peptides as well as a mouse IgG control, as shown in Supplementary Data Figure S2.

As a significant neuropathology is observed in the dentate gyrus of hAPOE4 mice as early as 6 months (54), we first asked whether the expression of human APOE4 protein exerted deleterious effects on OL and myelin fibers at younger ages. Using NeuN as a neuronal marker, we observed no decrease in neuronal density in neocortex of *Apoe*-KO, hAPOE3, or hAPOE4 relative to WT in mice ranging from 1 to 6 months of age (Fig. 3B, C). Myelin fiber density was also constant among all transgenic strains. In the neocortex (GM) and corpus callosum (WM), hAPOE4 genotype was not correlated with a reduction of MBP protein expression. In all genotypes, MBP immunostaining intensity increased in neocortex but decreased in corpus callosum from 1 to 6 months of age (Fig. 3D, F). The lack of change in the immunolabeling of myelin proteins, including MBP, MAG, and MOG in the neocortex of hAPOE3 and hAPOE4 mice was confirmed by Western blot (Fig. 3E, G). In contrast to the constancy of myelin proteins, we observed an age-dependent change in the OL population of neocortex (Fig. 3H–J), and corpus callosum (Fig. 3K–M). In the neocortex, we observed a gradual reduction of the number of Olig2$^+$ of all mice by 6 months. In the neocortex, the density of total OLs (Olig2$^+$) was reduced in hAPOE4 mice, even though the reduction did not reach statistical significance (Fig. 3I). By contrast, the number of myelinating CC1$^+$ mOLs increased in both *Apoe*-KO and WT mice between 1 and 6 months but remained relatively constant in hAPOE3 and hAPOE4 (Fig. 3J). The reduction in the density of CC1$^+$ mOLs was observed in both humanized transgenic mice but was statistically significant only in hAPOE4 neocortex at 6 months. In the corpus callosum, the number of Olig2$^+$ OLs increased in both *Apoe*-KO and WT mice but declined in hAPOE3 and hAPOE4 (Fig. 3M). An age-dependent increase in CC1$^+$ mOLs in corpus callosum was found in all strains up to 6 months of age in *Apoe*-KO and WT mice. In both hAPOE3 and hAPOE4 corpus callosum, CC1$^+$ mOLs numbers declined after 3 months, but the reduction did not reach statistical significance (Fig. 3M). Despite the reduced density, no apparent apoptotic Olig2$^+$ OLs or CC1$^+$ mOLs with pyknotic nuclei were observed in hAPOE4 mice. To ask if the lower mOL density in hAPOE4 mice led to reduced myelination in a more advanced stage, the neocortex and corpus callosum were histologically examined at 12 months (Fig. 4A). No difference in MBP myelinated area across neocortex and corpus callosum was detected between hAPOE3 and hAPOE4 mice. The myelinated area was similarly unchanged in the subregions of the neocortex (frontal, somatomotor, retrosplenial cortices) and corpus callosum (genu, splenium, and the associated fornix) as shown in Figure 4B, C.

Exogenous Human APOE4 Is Detrimental to mOLs In Vitro

The concordance of the histological findings in human and mouse tissues suggested that *APOE4* status was more significant than the more traditional pathognomonic measures of Alzheimer disease with respect to the effect on the OL population. To test our central hypothesis that APOE4-associated WM pathology is the immediate consequence of disrupted lipid metabolism in OL, we studied the effects of human APOE protein applied directly to primary cultures of OL derived from different transgenic mouse models in neuron-free microenvironments. Immunocytochemistry revealed that the primary OL culture derived from homozygous hAPOE3 and hAPOE4 mice exhibited no significant differences in the density of Olig2$^+$ population, nor its state of maturation (MBP$^+$ cells—Fig. 5A, B). This observation suggested that endogenous expression of hAPOE4 has no negative impact on the phenotype of OL-lineage cells in vitro. We then investigated the effects of APOE4 in cholesterol-depleted conditions using *Apoe*-KO-derived primary OL culture supplemented with Lovastatin (HMG-CoA inhibitor, 2.5 μM) with or without lipidated recombinant human APOE3 or APOE4 (rhAPOE3; rhAPOE4—Fig. 5C). Lovastatin significantly compromised the formation of MBP$^+$ mOL as well as the MBP$^+$ myelinated area in all conditions (Control, −55.5%; rhAPOE3, −64.3%; rhAPOE4 −48.5%, Fig. 5D, E). Lovastatin also significantly reduced the MAG$^+$ area, but not the percentage of MAG$^+$ mOL (Fig. 5D, F). Importantly, the application of rhAPOE4 throughout the differentiation period reduced the formation of MBP$^+$ mOL and MAG$^+$ mOL by 59.4% and 47.9% respectively, and reduced MBP$^+$ myelinated area by 70.6%, relative to control. Such deleterious effects were not observed after rhAPOE3 treatment alone (Fig. 5E, F). Among all measurements, the lowest numbers of MBP$^+$- and MAG$^+$-mOL were found with rhAPOE4 treatment following Lovastatin-mediated cholesterol depletion. To investigate if lipidated rhAPOE4 exert a gain-of-toxicity effect selectively on the mOL formation or in the entire OL lineage, the density of Olig2$^+$ population was quantified (Fig. 5G). While Lovastatin mediated significant reduction of Olig2 population, rhAPOE4, but not rhAPOE3, reduced Olig2$^+$ OLs by 15.1% in the absence of such cholesterol depletion. Furthermore, morphological analysis of the Olig2$^+$ nuclei showed that rhAPOE4, but not rhAPOE3, significantly reduced the nuclear size (area in

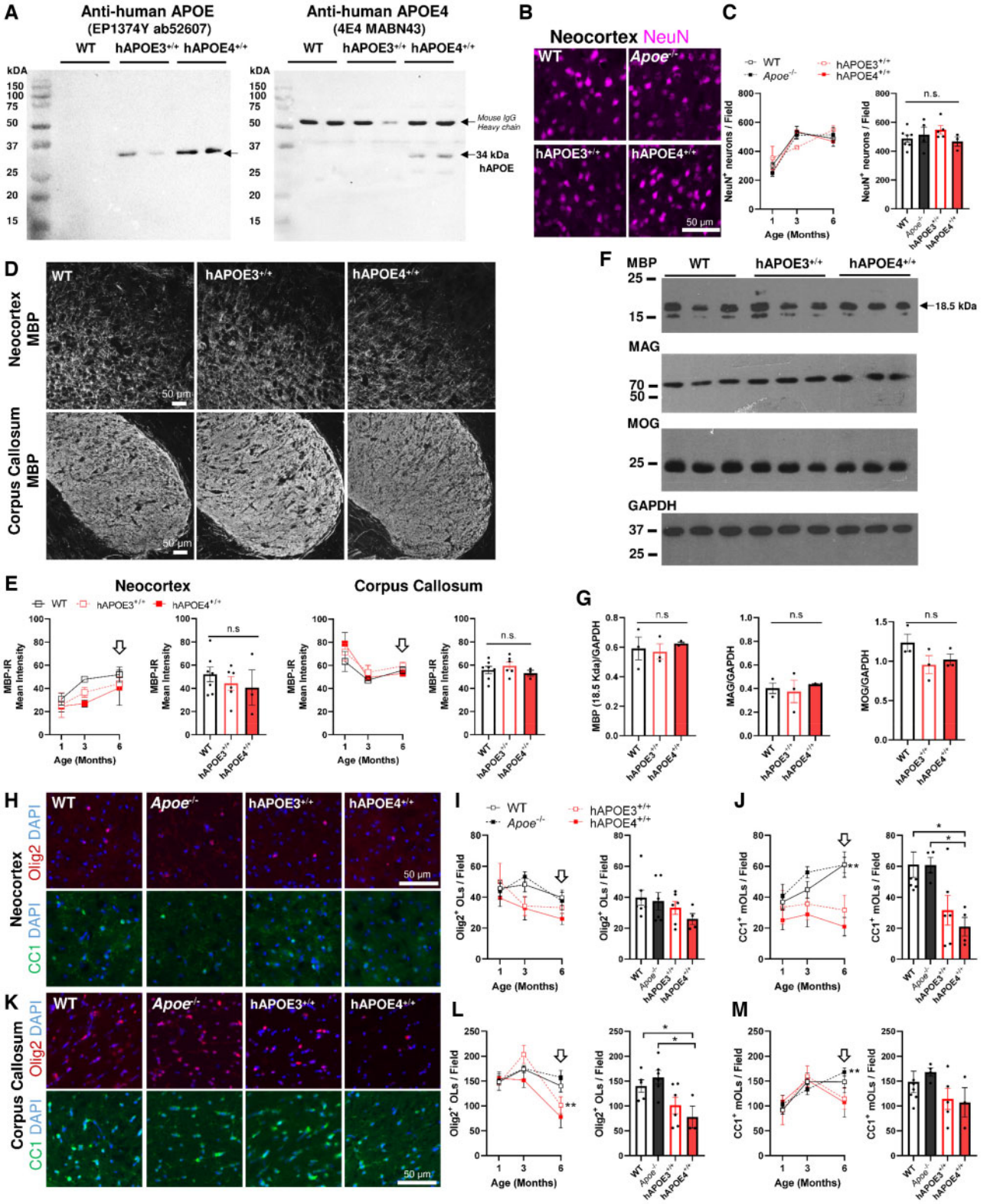

FIGURE 3. Age-dependent reduction of OLs but not myelin protein expression in hAPOE3 and hAPOE4 mouse models in vivo. **(A)** The expression of human total APOE and specific APOE4 protein in hAPOE4 mice was demonstrated by the detection by Clone EP1374Y (left) and Clone 4E4 (right) at 34 kDa, respectively (n = 3). Note that the bands above 50 kDa represent mouse IgG heavy chain in mouse brain tissue. For details, see Supplementary Data Figure S2. **(B)** Representative image of NeuN$^+$

μm^2) both in both nonmyelinating $Olig2^+$ OL and myelinating mOL population (Fig. 5H).

DISCUSSION

The loss of myelin content, myelinated tract integrity, and intracortical myelin fibers in the frontal lobe are frequently reported in neuroimaging studies of normal aging, with accelerated decline in sAD (10–13, 23–26, 28, 29). The current study helps to forge links between these systems-level changes and the cell biology of the aging and Alzheimer disease brain. We report that all stages of the OL lineage, up to and including the mOL population, are highly vulnerable to *APOE4* status, but minimally affected by the extent of Braak stages. In contrast, the total intracortical myelin area is slightly reduced with advancing Braak stage but appears to be independent of *APOE4* genotype. The lack of correlation between the decline of OL population and the extent of plaque and tangle pathology is consistent with our earlier report (30). Here, the postmortem human data suggested that the OL population is indeed more vulnerable to *APOE4* genotype than the classic AD pathology.

The longitudinal study of OL in the mouse brain validates and extends the human data. The myelination of human frontal cortex is said to follow an inverted U-shape, peaking at roughly 40 years of age (4). In mouse cortex, a hint of this temporal pattern was observed in the number of $Olig2^+$ cells, albeit the peak appears a younger relative age than would be expected from the human imaging data. This temporal discordance is likely explained by the fact that the 2 datasets are measuring different stages of OL development. Indeed, in contrast to the $Olig2^+$ data that measures the total number of cells in the lineage, the mature $CC1^+$ OL number continues to increase throughout the time period examined. One interpretation of these data is that the formation of new OPCs slows or stops with age, even as the existing population of precursors diminishes as they differentiate into mOL in support of the ongoing maturation of the nervous system. This model of the aging OL population is supported by the finding that, as in human brain, the overall level of myelin basic protein expression remains relatively constant in the aging mouse brain. The OL population in the humanized *APOE* transgenics initially attains normal numbers of both $Olig2^+$ and $CC1^+$ cells, which argues against a developmental defect. Yet an age-related decrease is seen in both precursors and mOLs suggesting that it is the maintenance of the myelinating population that is compromised by the replacement of mouse *Apoe* with human *APOE*. As the myelin sheath is continuously rejuvenated by the differentiation of OPCs after the degradation of mOLs (55, 56), we speculate that the gradual depletion of OPC subjects the mOL to an elevated demand for lipids in order to maintain normal levels of myelination. The unmet demands of lipids are likely part of the reasons for the observed compromise in myelin tract integrity in APOE4 carriers (27). At the tissue level, the density of myelin fibers remains unchanged in human APOE4 carriers and hAPOE4 mice despite the OL loss, but rhAPOE4 clearly reduced the size of myelin sheet formation per mOL in cell culture. It is plausible that while the unaltered myelin fiber density in human and mouse brain is found using classic MBP-based immunohistochemistry, an underlying shift of lipid content within the myelin sheath may occur in these fibers. Such biochemical change may result in the compromised myelin tract integrity commonly found in *APOE4* carriers (28). Recently, the use of high-throughput shotgun lipidomic analytics revealed an age-dependent alternation of lipid content in the corpus callosum of *Apoe*-deficient mice (57). While the present study suggests that APOE4 inhibits myelin formation in OLs, the possible effects of APOE4 on the lipid composition of myelin sheath generated by the sabotaged OLs warrants further investigation.

APOE4 is the strongest genetic risk factor for sAD and the ability of the APOE protein to carry the Aβ peptide has tied this lipid transport protein closely with the amyloid cascade hypothesis. However, in the fAD tissue, despite the remarkable disruption of intracortical myelin fibers by heavy amyloid plaque or extracellular neurofibrillary deposition, we found minimal reduction in the overall density of $Olig2^+$ cells. This suggests that the vulnerability of OL is independent of amyloid plaques. This argument is strengthened by the data from the hAPOE mice, which produce no amyloid plaques unless crossed with a transgenic strain carrying human amyloid

FIGURE 3. Continued
(magenta) cortical neurons among transgenic animals at 6 months. **(C)** The $NeuN^+$ neuron population increases with age, but no significant differences were found between the neocortex of WT, $Apoe^{-/-}$, hAPOE3, and hAPOE4 mice from 1 to 6 months. **(D)** Representative images of MBP in the neocortex (anterior cingulate) and corpus callosum (Genu) in WT, hAPOE3, and hAPOE4 mice at 6 months. **(E)** The immunoreactivity of the MBP signal increased in the neocortex but decreased in the corpus callosum among all mice from 1 to 6 months but no statistical differences were detected among the strains. Bar chart shows comparison at 6 months. **(F)** Consistent levels of myelin protein expression in the neocortex were confirmed by immunoblotting against MBP, MAG, and MOG with GAPDH as the loading control. **(G)** No statistical differences in myelin protein expression in the neocortex were detected between strains. **(H)** Representative images of $Olig2^+$ OLs (red) and $CC1^+$ mOLs in neocortex among all strains. **(I, J)** An age-dependent change of **(I)** total OL population ($Olig2^+$) and **(J)** mOL population ($CC1^+$) in neocortex between 1 and 6 months. The numbers of $CC1^+$ mOLs but not $Olig2^+$ OLs were only significantly reduced in hAPOE4 at 6 months (bar chart). **(K)** Representative images of $Olig2^+$ OLs (red) and $CC1^+$ mOLs in corpus callosum among all strains. **(L, M)** There was an age-dependent change of total OL population ($Olig2^+$) and mOL population ($CC1^+$) in corpus callosum between 1 and 6 months. The numbers of $Olig2^+$ OLs but not $CC1^+$ mOLs were significantly reduced in hAPOE4 at 6 months (Bar Chart). Statistical analysis by one-way ANOVA among groups with Tukey post hoc, or unpaired t-test between 2 groups (*$p < 0.05$, **$p < 0.01$, p value as indicated). Each time point contains at least 2 male and 2 female subjects with $n = 4–6$. No gender difference was found among all analyses.

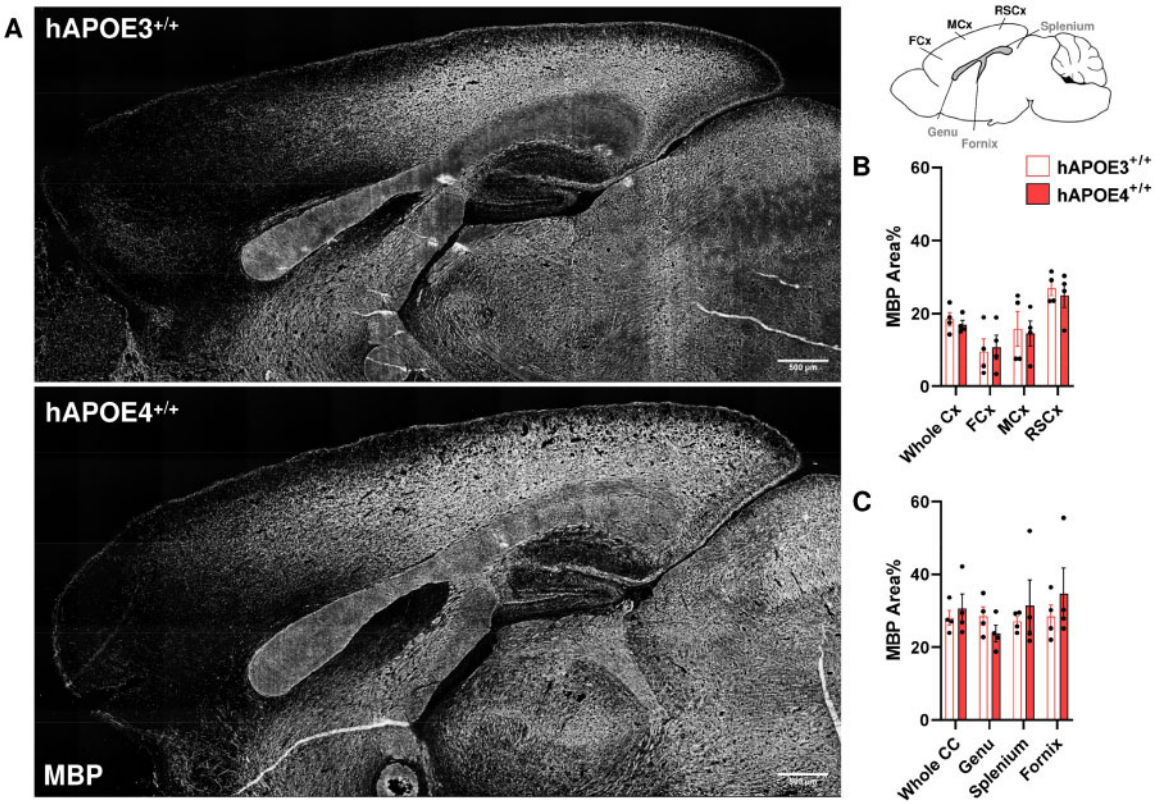

FIGURE 4. MBP-expressing myelin fibers remain unchanged at 12 months in hAPOE4. **(A)** Representative micrographs of MBP immunohistochemistry on the cerebrum of hAPO3 (above) and hAPOE4$^{+/+}$ (bottom) mice at 12 months. No observable abnormality was found. **(B, C)** Quantification of MBP^{+} myelinated area across the neocortex and corpus callosum was refined to subregions as denoted in the illustration on top right, but no significant differences were found. Whole Cx, average neocortex; FCx, frontal cortex; MCx, somatomotor cortex; RSCx, retrosplenial cortex; Whole CC, average corpus callosum.

precursor protein (51). The reduction of the OL population in hAPOE4 mice amid unaltered myelin density is likely the direct consequence of the defective physiological function of the human APOE4 protein. We also note that, unlike an earlier study on a similar strain of human *APOE* knock-in mice (54, 58), we found no signs of neurodegeneration in mice as old as 6 months of age. Although it is unknown whether silent neuronal pathology, such as synaptic loss, aberrant cell cycle reentry or cellular senescence, occurs at this stage, our finding suggests that APOE4-associated OL reduction is initiated prior to noticeable neuronal loss.

APOE protein is a well-known carrier that moves cholesterol and other lipids through the aqueous environment of the brain parenchyma, but this transport function is sabotaged by the amino acid changes of the APOE4 protein (17). Myelin is one of the most lipid-rich structures in the human brain. The data presented here lead us to hypothesize that *APOE4*-associated WM pathology is a more or less direct consequence of disrupted lipid metabolism. The construction of the myelin sheath requires abundant fatty acids and cholesterol that are normally synthesized by the OLs themselves (22, 59). With age, however, lipid synthesis in the OL declines, making it reliant on astrocyte-derived lipids to build and maintain normal levels of myelin (21). In primary OL culture, endogenous expression of human APOE3 or APOE4 in lieu of mouse *Apoe* has no effect on OL behavior. Yet, in the absence of endogenous APOE (*Apoe*$^{-/-}$), or in the presence of Lovastatin-mediated cholesterol-depletion, the addition of exogeneous lipidated human APOE4, but not APOE3 protein significantly compromised the formation of myelin. As reflected by the nuclear morphology analysis of OL in vitro, the reduced nuclear size by rhAPOE4 may be reflective of ongoing OL cell death process as in reports on neurodegenerative diseases (60, 61).

Taken together these data provide evidence that the negative effects of human APOE4 on OL function are due to its defective ability to transport lipids Indeed, APOE receptors such as low-density lipoprotein receptor (LDLR) and LDLR-related protein 1 (LRP1) are expressed by OLs. Furthermore, the deletion of LRP1 was shown to promote OL formation in vivo (62, 63). Our findings are consistent with these reports and suggested that APOE is crucial for OL maturation. It is conceivable that a complex relationship between human APOE isoforms and their receptor such as LRP1 may exist and impact on myelination in the aging brain. The critical nature of an adequate supply of lipids during myelination is also well illustrated by the strong upregulation of cholesterol synthesis gene pathway in experimental demyelination models (64), and rare genetic diseases with lipid metabolism dysfunctions (65). While it is plausible that age-related myelin degradation in human brain is a secondary event that follows

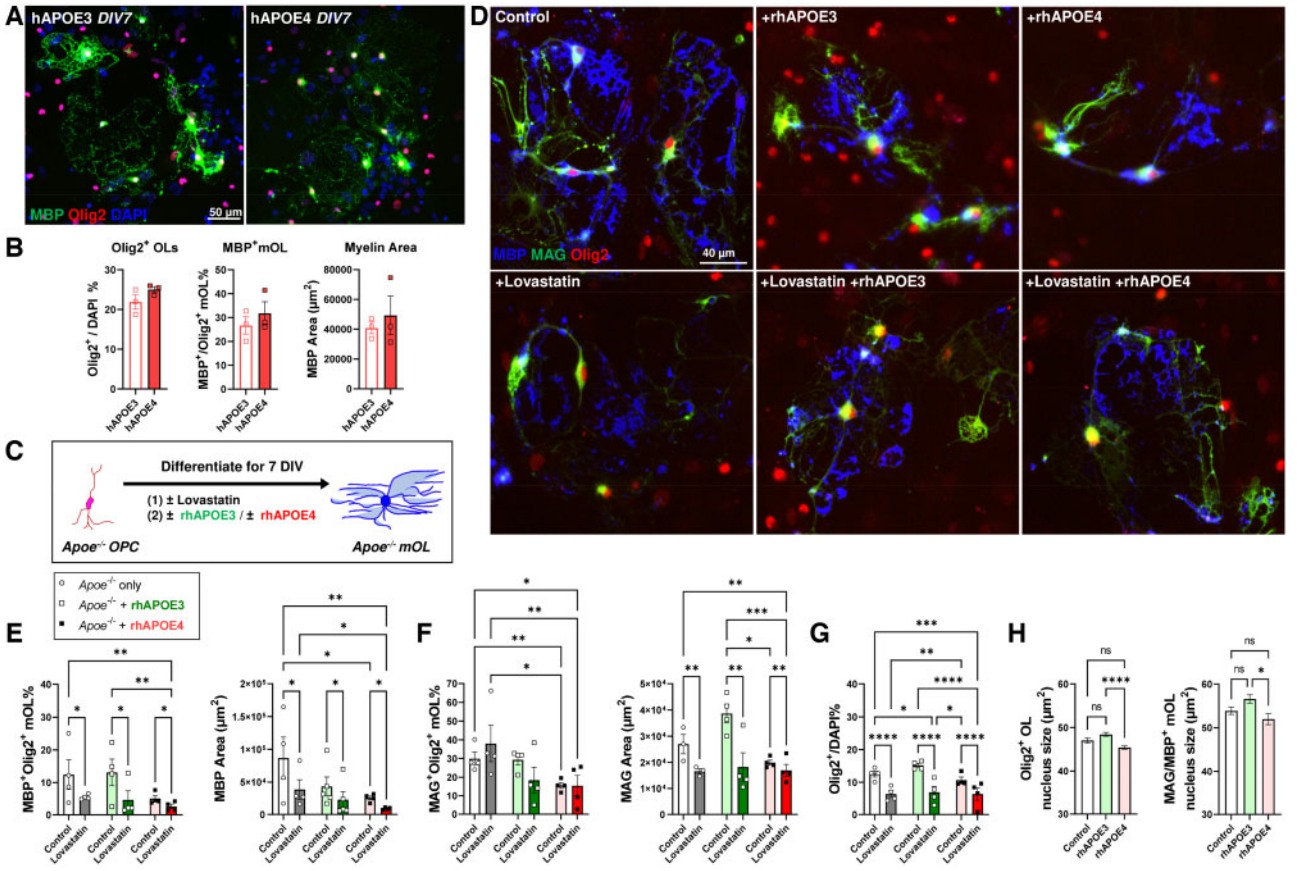

FIGURE 5. Recombinant human APOE4 protein exert direct deleterious effects on myelin-forming OL cell lines. **(A)** Representative image of immunocytochemistry on primary OL cell cultures at 7 DIV derived from homozygous hAPOE3 and hAPOE4 animals after differentiation at DIV 7 with MBP (green), Olig2 (red), and DAPI (blue). **(B)** Quantification revealed no differences in the formation of myelinating (MBP^+) in OL endogenously expressing hAPOE3 or hAPOE4. **(C)** Flowchart of experimental design to test the effects of lipidated rhAPOE3 and rhAPOE4 on OL differentiation in the absence of murine *Apoe* and intrinsic cholesterol supply. **(D)** Representative images of primary OL cell cultures at 7 DIV derived from $Apoe^{-/-}$mouse. $Apoe^{-/-}$ OPC (Olig2, red) undergo full differentiation and form myelinating OL expressing MBP (blue) and MAG (green). However, the formation of MBP^+ and MAG^+ was attenuated in the presence of Lovastatin-mediated cholesterol depletion as well as the addition of lipidated recombinant human APOE4 (rhAPOE4). **(E)** The MBP^+ mOL density and its myelinated area were significantly reduced by Lovastatin and/or rhAPOE4 treatment. **(F)** The MAG^+ mOL density and its myelinated area was also significantly reduced by Lovastatin and/or rhAPOE4 treatment, but not rhAPOE3 addition. **(G)** Quantifications of all $Olig2^+$ nuclei showed that Lovastatin significantly reduced the OL population. In the absence of Lovastatin, rhAPOE4 was associated with the lowest number of $Olig2^+$ cells. **(H)** rhAPOE4 alone was also associated with a significantly reduced nuclear size among nonmyelinating $Olig2^+$ OLs (left, at least 1664 cells analyzed per group) and fully differentiated MAG/MBP^+ mOLs (right, at least 326 cells analyzed per group) in control conditions from 4 independent experiments. Statistical analysis by two-way ANOVA among groups with Fisher least significant difference test between pairs (*$p < 0.05$, **$p < 0.01$, ***$p < 0.001$; ****$p < 0.0001$, $n = 4$ per group).

misfolded protein aggregation and neurofibrillary tangle formation during the aging process (14), our findings offer an alternative explanation, namely, that the APOE-associated effects on OL are related to its impact on lipid transport. The deleterious effect of APOE4 on OL lipid metabolism may lead to a higher burden of oxidative stress (66, 67) and subsequent DNA double strand break formation, ultimately leading to their demise (30, 68, 69).

Recently, activity-dependent myelin plasticity has been linked to memory formation (70–72). Experimentally enhanced myelination was also shown to restore or halt cognitive decline in a classic AD mouse model (73). These findings resonate with early neuroimaging findings of myelin loss in sAD brain and the tenets of the "Myelination-Hypothesis" as an explanation of the cognitive decline (2, 3, 74–81). Our findings offer a mechanistic link between the imaging results and the biochemistry of lipid transport. Coupled with genomic injury in OL (30, 69), the lack of membrane components may serve as a feed-forward amplification that offers a potential cellular mechanism for the myelin pathology in AD.

Conclusion

Both in vivo and in vitro evidence support the conclusion that human *APOE4* renders the OL population intrinsically susceptible to degeneration. This *APOE4*-associated OL degeneration is not secondary to amyloid deposition or to neuronal loss, but rather is closely related to problems associated with defective lipid transport. It is conceivable that *APOE4*-associated OL abnormalities may result in the shifts of lipid-protein composition in the myelin sheath and silent neuronal pathology, such as aberrant cell cycle re-entry or synaptic loss. These *APOE4* related events on myelin hypothesis at biochemistry and molecular level remain unexplored in the present study but warrants further investigations.

ACKNOWLEDGMENTS

We are in debt to the kind support from University of Pittsburgh ADRC (JK) for the postmortem human brain tissues. We are also grateful for the generous support from Dr Rada Koldamova and Dr Iliya Lefterov for their materials and reference mouse brain tissues during the pilot investigation that led to this study. We thank Ms Iris Ma Wai Ting for the technical support on genotyping and Ms Idy Wai Mei Wong for the technical support on slide scanning.

REFERENCES

1. Sherwood CC, Holloway RL, Semendeferi K, et al. Is prefrontal white matter enlargement a human evolutionary specialization? Nat Neurosci 2005;8:537–8; author reply 8
2. Bartzokis G, Beckson M, Lu PH, et al. Age-related changes in frontal and temporal lobe volumes in men: A magnetic resonance imaging study. Arch Gen Psychiatry 2001;58:461–5
3. Bartzokis G. Age-related myelin breakdown: A developmental model of cognitive decline and Alzheimer's disease. Neurobiol Aging 2004;25: 5–18; author reply 49–62
4. Bartzokis G, Cummings JL, Sultzer D, et al. White matter structural integrity in healthy aging adults and patients with Alzheimer disease: A magnetic resonance imaging study. Arch Neurol 2003;60:393–8
5. Walhovd KB, Fjell AM, Reinvang I, et al. Effects of age on volumes of cortex, white matter and subcortical structures. Neurobiol Aging 2005; 26:1261–70; discussion 75–78
6. Raz N, Lindenberger U, Rodrigue KM, et al. Regional brain changes in aging healthy adults: General trends, individual differences and modifiers. Cereb Cortex 2005;15:1676–89
7. Bartzokis G, Lu PH, Heydari P, et al. Multimodal magnetic resonance imaging assessment of white matter aging trajectories over the lifespan of healthy individuals. Biol Psychiatry 2012;72:1026–34
8. Bender AR, Raz N. Normal-appearing cerebral white matter in healthy adults: Mean change over 2 years and individual differences in change. Neurobiol Aging 2015;36:1834–48
9. Westlye LT, Walhovd KB, Dale AM, et al. Life-span changes of the human brain white matter: Diffusion tensor imaging (DTI) and volumetry. Cereb Cortex 2010;20:2055–68
10. Grydeland H, Walhovd KB, Tamnes CK, et al. Intracortical myelin links with performance variability across the human lifespan: Results from T1- and T2-weighted MRI myelin mapping and diffusion tensor imaging. J Neurosci 2013;33:18618–30
11. Walhovd KB, Fjell AM. White matter volume predicts reaction time instability. Neuropsychologia 2007;45:2277–84
12. Engvig A, Fjell AM, Westlye LT, et al. Memory training impacts short-term changes in aging white matter: A longitudinal diffusion tensor imaging study. Hum Brain Mapp 2012;33:2390–406
13. Lu PH, Lee GJ, Tishler TA, et al. Myelin breakdown mediates age-related slowing in cognitive processing speed in healthy elderly men. Brain Cogn 2013;81:131–8
14. Amlien IK, Fjell AM. Diffusion tensor imaging of white matter degeneration in Alzheimer's disease and mild cognitive impairment. Neuroscience 2014;276:206–15
15. Medina D, DeToledo-Morrell L, Urresta F, et al. White matter changes in mild cognitive impairment and AD: A diffusion tensor imaging study. Neurobiol Aging 2006;27:663–72
16. Michaelson DM. APOE epsilon4: The most prevalent yet understudied risk factor for Alzheimer's disease. Alzheimers Dement 2014;10:861–8
17. Yamazaki Y, Zhao N, Caulfield TR, et al. Apolipoprotein E and Alzheimer disease: Pathobiology and targeting strategies. Nat Rev Neurol 2019;15:501–18
18. Saher G, Stumpf SK. Cholesterol in myelin biogenesis and hypomyelinating disorders. Biochim Biophys Acta 2015;1851:1083–94
19. Maier O, De Jonge J, Nomden A, et al. Lovastatin induces the formation of abnormal myelin-like membrane sheets in primary oligodendrocytes. Glia 2009;57:402–13
20. Smolders I, Smets I, Maier O, et al. Simvastatin interferes with process outgrowth and branching of oligodendrocytes. J Neurosci Res 2010;88: 3361–75
21. Camargo N, Goudriaan A, van Deijk AF, et al. Oligodendroglial myelination requires astrocyte-derived lipids. PLoS Biol 2017;15:e1002605
22. Dimas P, Montani L, Pereira JA, et al. CNS myelination and remyelination depend on fatty acid synthesis by oligodendrocytes. Elife 2019;8: e44702
23. Bartzokis G, Lu PH, Geschwind DH, et al. Apolipoprotein E affects both myelin breakdown and cognition: Implications for age-related trajectories of decline into dementia. Biol Psychiatry 2007;62:1380–7
24. Ryan L, Walther K, Bendlin BB, et al. Age-related differences in white matter integrity and cognitive function are related to APOE status. Neuroimage 2011;54:1565–77
25. Operto G, Cacciaglia R, Grau-Rivera O, ALFA Study, et al. White matter microstructure is altered in cognitively normal middle-aged APOE-epsilon4 homozygotes. Alzheimers Res Ther 2018;10:48
26. Operto G, Molinuevo JL, Cacciaglia R, ALFA Study, et al. Interactive effect of age and APOE-epsilon4 allele load on white matter myelin content in cognitively normal middle-aged subjects. Neuroimage Clin 2019; 24:101983
27. Tse KH, Herrup K. Re-imagining Alzheimer's disease – The diminishing importance of amyloid and a glimpse of what lies ahead. J Neurochem 2017;143:432–44
28. Rieckmann A, Van Dijk KR, Sperling RA, et al. Accelerated decline in white matter integrity in clinically normal individuals at risk for Alzheimer's disease. Neurobiol Aging 2016;42:177–88
29. Adluru N, Destiche DJ, Lu SY, et al. White matter microstructure in late middle-age: Effects of apolipoprotein E4 and parental family history of Alzheimer's disease. Neuroimage Clin 2014;4:730–42
30. Tse KH, Cheng A, Ma F, et al. DNA damage-associated oligodendrocyte degeneration precedes amyloid pathology and contributes to Alzheimer's disease and dementia. Alzheimers Dement 2018;14:664–79
31. Braak H, Alafuzoff I, Arzberger T, et al. Staging of Alzheimer disease-associated neurofibrillary pathology using paraffin sections and immunocytochemistry. Acta Neuropathol 2006;112:389–404
32. Consensus recommendations for the postmortem diagnosis of Alzheimer's disease. The National Institute on Aging, and Reagan Institute Working Group on Diagnostic Criteria for the Neuropathological Assessment of Alzheimer's Disease. Neurobiol Aging 1997;18:S1–2
33. Hamanaka H, Katoh-Fukui Y, Suzuki K, et al. Altered cholesterol metabolism in human apolipoprotein E4 knock-in mice. Hum Mol Genet 2000; 9:353–61
34. Calero O, Hortiguela R, Bullido MJ, et al. Apolipoprotein E genotyping method by real time PCR, a fast and cost-effective alternative to the TaqMan and FRET assays. J Neurosci Methods 2009;183:238–40
35. Walker L, McAleese KE, Thomas AJ, et al. Neuropathologically mixed Alzheimer's and Lewy body disease: Burden of pathological protein aggregates differs between clinical phenotypes. Acta Neuropathol 2015; 129:729–48
36. Calero O, Garcia-Albert L, Rodriguez-Martin A, et al. A fast and cost-effective method for apolipoprotein E isotyping as an alternative to APOE genotyping for patient screening and stratification. Sci Rep 2018; 8:5969

37. Veiga S, Rodriguez-Martin A, Garcia-Ribas G, et al. Validation of a novel and accurate ApoE4 assay for automated chemistry analyzers. Sci Rep 2020;10:2138
38. Bankhead P, Loughrey MB, Fernandez JA, et al. QuPath: Open source software for digital pathology image analysis. Sci Rep 2017;7:16878
39. Emery B, Dugas JC. Purification of oligodendrocyte lineage cells from mouse cortices by immunopanning. Cold Spring Harb Protoc 2013;2013: 854–68
40. Luo F, Zhang J, Burke K, et al. The activators of cyclin-dependent kinase 5 p35 and p39 are essential for oligodendrocyte maturation, process formation, and myelination. J Neurosci 2016;36:3024–37
41. Tse KH, Cheng A, Ma F, et al. DNA damage-associated oligodendrocyte degeneration precedes amyloid pathology and contributes to Alzheimer's disease and dementia. Alzheimers Dement 2018;14:664–679.
42. Wang H, Kulas JA, Wang C, et al. Regulation of beta-amyloid production in neurons by astrocyte-derived cholesterol. Proc Natl Acad Sci U S A 2021;118:e2102191118
43. Lee S, Lee DK. What is the proper way to apply the multiple comparison test? Korean J Anesthesiol 2018;71:353–60
44. Rothman KJ. No adjustments are needed for multiple comparisons. Epidemiology 1990;1:43–6
45. Li F, Ayaki T, Maki T, et al. NLRP3 inflammasome-related proteins are upregulated in the putamen of patients with multiple system atrophy. J Neuropathol Exp Neurol 2018;77:1055–65
46. Levin JR, Serlin RC, Seaman MA. A controlled, powerful multiple-comparison strategy for several situations. Psychol Bull 1994;115:153–9
47. Nieuwenhuys R. The myeloarchitectonic studies on the human cerebral cortex of the Vogt-Vogt school, and their significance for the interpretation of functional neuroimaging data. Brain Struct Funct 2013;218: 303–52
48. Bujalka H, Koenning M, Jackson S, et al. MYRF is a membrane-associated transcription factor that autoproteolytically cleaves to directly activate myelin genes. PLoS Biol 2013;11:e1001625
49. Hornig J, Frob F, Vogl MR, et al. The transcription factors Sox10 and Myrf define an essential regulatory network module in differentiating oligodendrocytes. PLoS Genet 2013;9:e1003907
50. Hayashi H, Igbavboa U, Hamanaka H, et al. Cholesterol is increased in the exofacial leaflet of synaptic plasma membranes of human apolipoprotein E4 knock-in mice. Neuroreport 2002;13:383–6
51. Mann KM, Thorngate FE, Katoh-Fukui Y, et al. Independent effects of APOE on cholesterol metabolism and brain Abeta levels in an Alzheimer disease mouse model. Hum Mol Genet 2004;13:1959–68
52. Morishima-Kawashima M, Han X, Tanimura Y, et al. Effects of human apolipoprotein E isoforms on the amyloid beta-protein concentration and lipid composition in brain low-density membrane domains. J Neurochem 2007;101:949–58
53. Nishitsuji K, Hosono T, Nakamura T, et al. Apolipoprotein E regulates the integrity of tight junctions in an isoform-dependent manner in an in vitro blood-brain barrier model. J Biol Chem 2011;286:17536–42
54. Tong LM, Yoon SY, Andrews-Zwilling Y, et al. Enhancing GABA signaling during middle adulthood prevents age-dependent GABAergic interneuron decline and learning and memory deficits in ApoE4 mice. J Neurosci 2016;36:2316–22
55. Franklin RJM, Frisen J, Lyons DA. Revisiting remyelination: Towards a consensus on the regeneration of CNS myelin. Semin Cell Dev Biol 2020;116:3–9.
56. Duncan ID, Radcliff AB, Heidari M, et al. The adult oligodendrocyte can participate in remyelination. Proc Natl Acad Sci U S A 2018;115: E11807–16
57. Fitzner D, Bader JM, Penkert H, et al. Cell-type- and brain-region-resolved mouse brain lipidome. Cell Rep 2020;32:108132
58. Leung L, Andrews-Zwilling Y, Yoon SY, et al. Apolipoprotein E4 causes age- and sex-dependent impairments of hilar GABAergic interneurons and learning and memory deficits in mice. PLoS One 2012;7:e53569
59. Saher G, Brugger B, Lappe-Siefke C, et al. High cholesterol level is essential for myelin membrane growth. Nat Neurosci 2005;8:468–75
60. Gagyi E, Kormos B, Castellanos KJ, et al. Decreased oligodendrocyte nuclear diameter in Alzheimer's disease and Lewy body dementia. Brain Pathol 2012;22:803–10
61. Uyama N, Uchihara T, Mochizuki Y, et al. Selective nuclear shrinkage of oligodendrocytes lacking glial cytoplasmic inclusions in multiple system atrophy: A 3-dimensional volumetric study. J Neuropathol Exp Neurol 2009;68:1084–91
62. Xie Y, Zhang X, Xu P, et al. Aberrant oligodendroglial LDL receptor orchestrates demyelination in chronic cerebral ischemia. J Clin Invest 2021;131:e128114
63. Auderset L, Pitman KA, Cullen CL, et al. Low-density lipoprotein receptor-related protein 1 (LRP1) is a negative regulator of oligodendrocyte progenitor cell differentiation in the adult mouse brain. Front Cell Dev Biol 2020;8:564351
64. Voskuhl RR, Itoh N, Tassoni A, et al. Gene expression in oligodendrocytes during remyelination reveals cholesterol homeostasis as a therapeutic target in multiple sclerosis. Proc Natl Acad Sci U S A 2019;116: 10130–9
65. Chrast R, Saher G, Nave KA, et al. Lipid metabolism in myelinating glial cells: Lessons from human inherited disorders and mouse models. J Lipid Res 2011;52:419–34
66. Tracey TJ, Steyn FJ, Wolvetang EJ, et al. Neuronal lipid metabolism: Multiple pathways driving functional outcomes in health and disease. Front Mol Neurosci 2018;11:10
67. Back SA, Gan X, Li Y, et al. Maturation-dependent vulnerability of oligodendrocytes to oxidative stress-induced death caused by glutathione depletion. J Neurosci 1998;18:6241–53
68. Tse K-H, Cheng A, Yeung SH-S, et al. Myelin pathology in ataxia-telangiectasia is the cell-intrinsic consequence of ATM deficiency in the oligodendrocytes. medRxiv (PrePrint) 2021. https: //doi.org/10.1101/2021.01.22.20245217.
69. Tse KH, Herrup K. DNA damage in the oligodendrocyte lineage and its role in brain aging. Mech Ageing Dev 2017;161:37–50
70. Hill RA, Li AM, Grutzendler J. Lifelong cortical myelin plasticity and age-related degeneration in the live mammalian brain. Nat Neurosci 2018;21:683–95
71. Fields RD. A new mechanism of nervous system plasticity: Activity-dependent myelination. Nat Rev Neurosci 2015;16:756–67
72. Wang F, Ren SY, Chen JF, et al. Myelin degeneration and diminished myelin renewal contribute to age-related deficits in memory. Nat Neurosci 2020;23:481–6
73. Chen JF, Liu K, Hu B, et al. Enhancing myelin renewal reverses cognitive dysfunction in a murine model of Alzheimer's disease. Neuron 2021;109:2292–307.e5
74. Bartzokis G, Lu PH, Tingus K, et al. Lifespan trajectory of myelin integrity and maximum motor speed. Neurobiol Aging 2010;31:1554–62
75. Bartzokis G, Sultzer D, Lu PH, et al. Heterogeneous age-related breakdown of white matter structural integrity: Implications for cortical "disconnection" in aging and Alzheimer's disease. Neurobiol Aging 2004;25:843–51
76. Benes FM. A disturbance of late myelination as a trigger for Alzheimer's disease. Neurobiol Aging 2004;25:41–3
77. Connor JR. Myelin breakdown in Alzheimer's disease: A commentary. Neurobiol Aging 2004;25:45–7
78. Braak H, Del Tredici K. Poor and protracted myelination as a contributory factor to neurodegenerative disorders. Neurobiol Aging 2004;25: 19–23
79. Jernigan TL, Fennema-Notestine C. White matter mapping is needed. Neurobiol Aging 2004;25:37–9
80. Noble M. The possible role of myelin destruction as a precipitating event in Alzheimer's disease. Neurobiol Aging 2004;25:25–31
81. Whitman GT, Cotman CW. Oligodendrocyte degeneration in AD. Neurobiol Aging 2004;25:33–6